PHENOMENA AFFECTING USED NUCLEAR FUEL CLADDING TEMPERATURES DURING VACUUM DRYING OPERATIONS

Hadj-Nacer M. [*1], Manzo T.[1], Ho M. [2], Graur I. [2] and Greiner M. [1]
[1] *University of Nevada Reno, 1664 N. Virginia St. Reno, 89557 Nevada, USA.*
[2] *Aix-Marseille Université, Polytech Marseille, UMR CNRS 7343, 5 rue Enrico Fermi, 13453 Marseille Cedex 13, France*
[*] *mhadjnacer@unr.edu*

A two-dimensional computational model of a loaded used nuclear fuel canister filled with helium gas was constructed to predict the cladding temperature during vacuum drying conditions. It includes distinct regions for the fuel pellets, cladding and helium within each basket opening. Symmetry boundary conditions are employed so that only one-eighth of the package cross-section is included, and temperature boundary conditions on the canister exterior surface in contact with water is used. Thermal modeling includes heat generation within the fuel pellets, conduction heat transfer within all solid components, and conduction and surface-to-surface radiation across the gas filled regions. The peak clad temperature is determined as a function of fuel heat generation rate, assuming atmospheric pressure helium. The allowable fuel heat generation rate, which brings the peak clad temperature to its limit is determined. The Willis solid/gas interfaces thermal-resistance model is verified against discrete-velocity-method slip-region rarefied-gas heat transfer calculated across planar and cylindrical helium filled-gaps for a range of thermal accommodation coefficients, α. The Willis model is then implemented at the solid/gas interfaces within the canister model. Simulations with a helium pressure of 100 Pa and α = 1, 0.4 and 0.2 are preformed to determine how much hotter the fuel cladding is under vacuum drying conditions compared to atmospheric pressure. The results showed that the allowed fuel heat generation rate is reduced by up to 34% for α = 0.2. Transient simulations are performed, and show that the fuel cladding temperature rises for roughly 50 hours after the loaded canister is removed from the water pool.

I. INTRODUCTION

Following discharge from the reactor, used nuclear fuel is stored in a water-filled pool for many years, where decay heat is transported by the water [1]. After appropriate time, typically five years or more, the used fuel is loaded from the storage pool into a canister that was earlier placed in a transfer cask and both lowered into the pool. The lid is then installed and the transfer cask is lifted out of the pool and drained [2]. Small amounts of water may remain at the bottom and in the crevices of the canister or adsorbed to the cladding surfaces [3]. The presence of residual water within a sealed dry-storage cask may result in container pressurization, fuel retrievability issues, container and fuel cladding corrosion and/or formation of combustible mixtures of hydrogen and oxygen during transport and long-term storage [4]. After drying, the canister is backfilled with helium nitrogen to a pressure between 3 and 7 atm, then is sealed and the final cover lid is bolted or welded in place.

With the absence of a defined used-fuel disposal and/or reprocessing path, it is crucial to assure the safety of long-term dry cask storage systems [5]. Federal regulations (10CFR72) requires that "spent fuel cladding must be protected during storage against degradation that leads to gross ruptures or the fuel must be otherwise confined such that degradation of the fuel during storage will not pose operational safety problems with respect to its removal from storage." The cladding is the primary confinement barrier for the used fuel pellets and fission gas. Its integrity must be protected to assure that, after decades in storage, the assemblies can be safely transferred to other packages, and/or transported to other locations. Radial hydride formation within the cladding has the potential to radically reduce cladding ductility and its suitability for transport or long term storage [5].

During all post-reactor drying, transfer, storage and transport operations the fuel cladding must be kept below the temperature limit of 400°C (673K), specified by the Nuclear Regulatory Commission Interim Staff Guidance-11, Revision 3 (ISG-11) [6], to avoid (a) dissolution of circumferential hydrides that exist in the cladding and (b) high gas pressures within the tubes, which leads to high cladding hoop stress [6]. If these hydrides dissolve and the hoop stresses become large, then as the heat generation of the used fuel decreases during long-term storage radial hydrides may form and cause the cladding to become brittle [7-10]. Drying operations [11] may be the most likely event to cause the fuel temperature to exceed the temperature limit. This is because drying is the first operation when the fuel is removed from water and placed in a gas-filled environment, while the fuel heat generation is still relatively high.

Currently, two methods are used by industry to remove moisture and residual water from the canister, forced helium dehydration and vacuum drying.

Forced helium dehydration is used for high burnup or other high heat generation fuels. Dry helium is forced through a port near the top of the canister and withdrawn through a tube that reaches its bottom. Moisture is removed from the helium by condensing, demoisturizing, and preheating the gas outside the canister. The process continues until the technical specification, for the temperature of helium exiting the system demoisturizer is

maintained below 21°F (-6°C) for a minimum 30 minutes, [1, 11] is reached to consider that the canister is dry. This method requires several pieces of equipment (gas demoisturizing and cooling system) to accomplish the process.

Vacuum drying method requires less equipment compared to the forced helium dehydration. During this method a vacuum drying system is connected to the canister and the pressure in the canister is decreased as low as 70 Pa to promote evaporation and removal of water. Several cycles of evacuation and refill are accomplished until the technical specifications of maintaining a low pressure of 400 Pa (3 Torr) for 30 minutes are fulfilled [2, 11]. Because of the low pressures and densities associated with vacuum drying, buoyancy-induced gas motion and natural convection heat transfer from the fuel to the solid surfaces of the canister is small and can be neglected. The gas thermal conductivity is almost same as it is at atmospheric pressure conditions. Moreover, the rarefaction condition (low pressure) induces a notable temperature difference (temperature jump) between the fuel cladding wall and the gas that is interacting with it [12-14]. As the pressure increases this temperature jump becomes negligible, but the more rarefied the gas is the more important this temperature jump is and may contribute to higher cladding temperatures during the vacuum drying process compared to atmospheric pressure conditions.

Currently, package vendors predict cladding temperatures and the resulting hoop stresses during drying operation using experimentally-benchmarked whole-package CFD simulations [1, 15-17]. In these models, the fuel and basket are replaced by a region with an effective thermal conductivity and porosity, which are calculated without regard to the rarefied-gas temperature-jump thermal resistance. However, the fuel heat generation in the tests used to validate the current methods was moderately low. The effect of the rarified-gas thermal resistance on peak cladding temperatures increases with heat generation rate.

Current Work: The objective of this work is to develop CFD simulations that accurately predict used nuclear fuel peak cladding temperatures during the vacuum drying operations. The ANSYS/Fluent CFD package is used to model heat transfer across the fuel package. The simulations are performed using the temperature jump condition at the interfaces between rarefied gases and solid surfaces. In order to benchmark the ANSYS/Fluent simulation technique, conduction heat transfer simulations through rarefied helium gas in a gap between parallel plates and concentric cylinders are performed for a solid surface temperature difference of 30°C and gas pressures from 10^5 to 10 Pa. These results are compared to the gas kinetic model calculations. The benchmarked ANSYS/Fluent simulations are then used to predict the cladding temperature within a loaded transfer cask for a range of fuel heat generation rates. Simulations are performed using a continuum model for helium at pressure of 1 atm (~10^5 Pa), and temperature jump model for helium at 100 Pa. The fuel heat generation rates that bring the cladding temperature to ISG-11 limit temperature of 400°C [6], and a reduced limit of 370°C [18] used in Germany, are reported. The transient response of the fuel package subjected to vacuum drying operation is also examined. The time required to reach the ISG limit is reported.

II. RARIFIED GAS HEAT TRANSFER

At low pressure conditions the number of collisions between gas molecules and solid surfaces is low comparing to the normal atmospheric conditions. The continuity of the macroscopic parameters of temperature and velocity near the wall is not achieved. At these pressures some special characteristics related to the gas rarefaction can be observed. The principal parameter characterizing rarefied gas is the Knudsen number (Kn), which is defined as

$$Kn = \frac{\lambda}{Lc} \tag{1}$$

where, λ is the mean free path defined as the distance travelled by molecules between two successive collisions [19] and Lc is a representative physical length scale. Typically the characteristic length Lc is the smallest dimension of the system. The mean free path λ is defined as

$$\lambda = \frac{\mu}{P}\sqrt{\frac{2k_B T}{m}} \tag{2}$$

where, P and T are the pressure and the temperature, respectively. k_B is the Boltzmann's constant, m is the mass of the gas molecule, and μ is the dynamic viscosity, whose temperature dependence is determined using the Hard Sphere (HS) model as

$$\mu = \mu_0\left(\frac{T}{T_0}\right)^{1/2} \tag{3}$$

where, T_0 is the reference temperature equal to 273.15 K and μ_0 is the reference viscosity that depends on the gas, equal to 1.865×10^{-5} Pa·s for helium.

The Knudsen number is used as a parameter to describe the gas rarefaction level. Using this parameter we can distinguish four regimes of rarefaction; (i) The continuum regime ($Kn\leq10^{-3}$), where the flow and heat transfer can be accurately modeled using the classical Navier-Stokes and Convective Energy equations. The number of collisions is big enough to reach the continuity of parameters at the wall. (ii) The slip regime ($10^{-3}\leq Kn\leq10^{-1}$), where the number of collisions molecules-surface are not enough to reach equilibrium near the wall, but far from the wall equilibrium is reached. In this regime the Navier-Stokes and Convective Energy equations are still appropriate but they should be subjected to the conditions of velocity-slip and temperature-jump at the wall. (iii) Transitional regime ($10^{-1}<Kn<10$), it is the most

difficult regime for modeling. In this regime the mean free path is comparable to the characteristic length scale, therefore, the collisions between molecules and surfaces dominate the collisions between molecules. To model the flow in this regime the Boltzmann equation should be solved using the Discrete Velocity Method (DVM) [20] or Direct Simulation Monte Carlo (DSMC) method [21]. (iv) The free molecular regime ($10 \leq Kn$), where the gas is highly rarefied and the flow is driven by the collisions between molecules and surface. In this regime the flow is modeled using the collisional kinetic Boltzmann equation.

It should be pointed out that all the regimes cited above can be accurately modelled using the kinetic theory, by solving the Boltzmann equation. Nevertheless, it is inefficient to implement this equation or other kinetic equations for gas flow simulation in the hydrodynamic and slip regimes because of the large computational efforts needed for their solution.

II.A. Thermal accommodation coefficient

Under rarefied conditions, the collisions between gas molecules and surfaces dominate the molecules-molecules collisions. Maxwell [22] postulated that when molecules enter in collision with the wall there are two possibilities: (i) the molecules can be reflected specularly, without transferring any of their momentum or energy to the surface (the molecule's temperature and tangential velocity remain unchanged, but its velocity normal to the wall is reversed), and (ii) the molecules can be reflected diffusely: a molecule leaving the surface "forgets" all information about upon collision and it leaves accommodating the surface properties (i.e., their average bulk velocity is equal to the surface velocity and the temperature is equal to the temperature of the surface). Based on this definition, the Thermal Accommodation Coefficient (TAC), denoted here by α, can be related to the temperature of incident T_i and reflected T_r molecules as [23]

$$\alpha = \frac{T_i - T_r}{T_i - T_w} \tag{4}$$

where T_w is the wall temperature. The value of TAC is in the range from 0 to 1. In the case of α=0, the reflection is perfectly specular. For α=1, the incident molecule is reflected diffusely after complete accommodation to the wall temperature. When α is between 0 and 1, the fraction of molecules equal to (1-α) is reflected specularly and the fraction of molecules equal to α is reflected diffusely.

The values of TAC were determined experimentally for a wide range of surfaces and gas molecules, using different methods [23-24]. Its value depends on a number of parameters, such as the type of gas, surface material, its cleanliness and its roughness. Song and Yovanovich [24] reported values of α close to 1 for heaviest molecules and values close to 0 for lighter molecules. The value of TAC reported for the pair helium-stainless steel [24] is in the range [0.2, 0.4] depending on temperature. The values α=1, 0.4 and 0.2 will be used in the current work for all the calculations.

II.B. Temperature jump model

In slip regime ($10^{-3} \leq Kn \leq 10^{-1}$), the interaction between molecules and wall is not sufficient to reach the equilibrium of temperature near the wall, *i.e.* $T_g \neq T_w$. The local temperature-difference or temperature-jump between the gas and wall can be determined using a resistance model [25],

$$T_g - T_w = \zeta_T \lambda \frac{\partial T_g}{\partial r} = R_{TJ} Q \tag{5}$$

In this model, Q is the portion of the heat transfer rate transported by conduction within the surrounding gas and does not include the component transported by radiation to other surfaces. The temperature-jump thermal-resistance is

$$R_{TJ} = \frac{\lambda \zeta_T}{A\kappa} \tag{6}$$

In this expression A is the boundary surface area, and κ is the gas thermal conductivity that is related to the viscosity μ (Eq. 3), the gas specific heat at constant pressure c_P and Prandtl number Pr as

$$\kappa = \frac{c_P}{\Pr} \mu \tag{7}$$

In equation (6) ζ_T is the temperature jump coefficient. Lin and Willis, 1972 [26] proposed an expression for this coefficient using the Bhatnagar-Gross-Krook (BGK) kinetic model. This expression reads

$$\zeta_T = \frac{\sqrt{\pi}\gamma}{(\gamma+1)\Pr}\left(\frac{2-\alpha}{\alpha} + 0.17\right) \tag{8}$$

where γ is the ratio of specific heat at constant pressure to that at constant volume. The temperature jump coefficient in Equation (8) is a function of TAC (α). A lower value of α will lead to a higher temperature jump between the wall and gas molecules interacting with it.

III. BENCHAMRK SIMULATIONS

Figure 1 shows the two-dimensional computational domain of the planar and annual regions used in the current work to benchmark ANSYS/Fluent simulations of conduction through rarefied gases. The planar region (Fig. 1a) consists of two parallel plates spaced by gap H=10 mm. The length L of the plates was set to 100 times the gap H to neglect the lateral walls effect. For the annular region (Fig. 1b) the inner and outer cylinders radii are R_A=5 mm and R_B=10 mm, respectively. The hot and cold temperature of the surfaces for both geometries are respectively, T_A=330K and T_B=300K. These spacings and temperature differences were chosen because they are similar to those between the fuel rods within used fuel assemblies.

Graur et al [20] used the kinetic Shakhov model (S-model) equations to solve the Boltzmann equation in

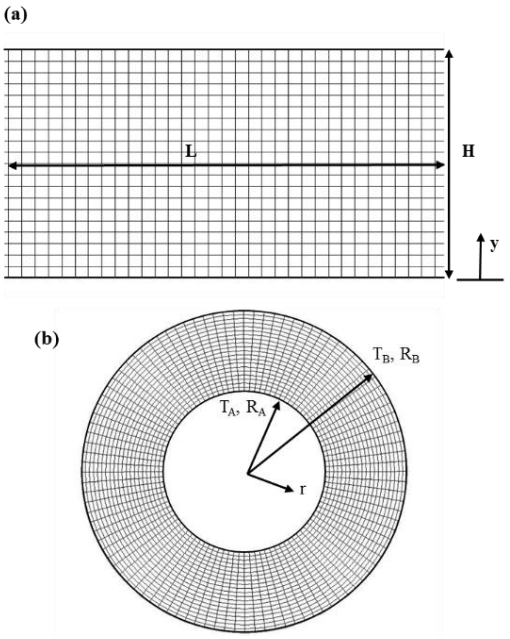

Fig. 1. Benchmark computational domains (a) Planar region between parallel plates (b) Annular region between concentric cylinders.

plannar and annular regions using the DVM subjected to the Maxwellian specular-diffuse boundary conditions. The Hard Sphere (HS) intermolecular interaction model was used for viscosity calculation (Eq. 3). The heat flux across the planar and annular gaps was calculated for different values of the accommodation coefficients.

Figures 2a and 2b show the comparison between the heat transfer reduction ratio $(Q_C\text{-}Q)/Q_C$, where Q_C is the heat flux limit in the continuum regime, obtained from Fluent simulations using the Willis temperature jump model (Eq. 9) and from the S-model kinetic equation for different values of the thermal accommodation coefficient α.

From these figures (2a and 2b) one can see that the ANSYS/Fluent simulations are in good agreement with the DVM kinetic calculations for both configurations (parallel plates and concentric cylinders) and for all the values of the thermal accommodation coefficient (α=1, 0.4 and 0.2). The maximum deviation of the Fluent model from the kinetic calculations is less than 1.1% for the concentric cylinders configuration. For the parallel plate configuration the maximum deviation of 2.4% is observed for pressure of 22 Pa (corresponding to the limit of the slip regime) and thermal accommodation coefficient of 0.2. For the other values of the thermal accommodation coefficient the deviation was smaller than 1.26%.

From Figures 2 it is clear that the Fluent model was able to predict with a good accuracy the conduction heat transfer in the slip regime. In the next section, ANSYS/Fluent simulations with the Willis temperature jump model will be performed to calculate the peak cladding temperature in a whole package model.

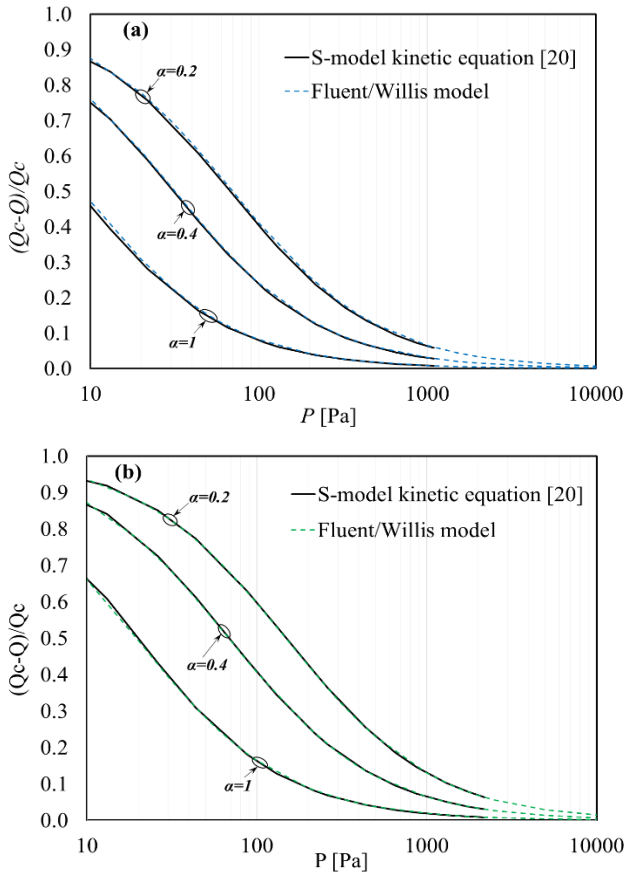

Fig. 2. Heat transfer reduction ratio as function of gas pressure and thermal accommodation coefficient (a) Planar region between parallel plates (b) Annular Region between concentric cylinders.

IV. TRANSFER CASK MODEL

Figure 3 shows the computational-domain-material-regionals of the canister used in ANSYS/Fluent simulations. The model presented in Figure 3 is similar to the Transnuclear TN-24 canister that contains 24 PWR Westinghouse fuel assemblies. This model uses symmetry to simplify the complete package into a one-eighth model.

The domain shown in Figures 3a, 3b and 3c includes a square array of 15x15 fuel rods with an UO_2 core surrounded by a Zircaloy sheath. Instrumentation rods are included in the model and are assumed similar size to the fuel rods. The square fuel rod assembly is centered inside a stainless steel basket. The stainless steel basket rests inside the aluminum supports along with the neutron poison; thermal properties for BORAL® were used for the neutron poison. The neutron poison is placed in selected spots inside the aluminum support geometry. In Figure 3b, a detailed view of the fuel rod array showing the gas filled regions of the instrumentation rods between the aluminum support and the stainless steel which is in a symmetrical pattern. Figure 3c shows the gap between the aluminum support and the stainless-steel-enclosure which is gas filled

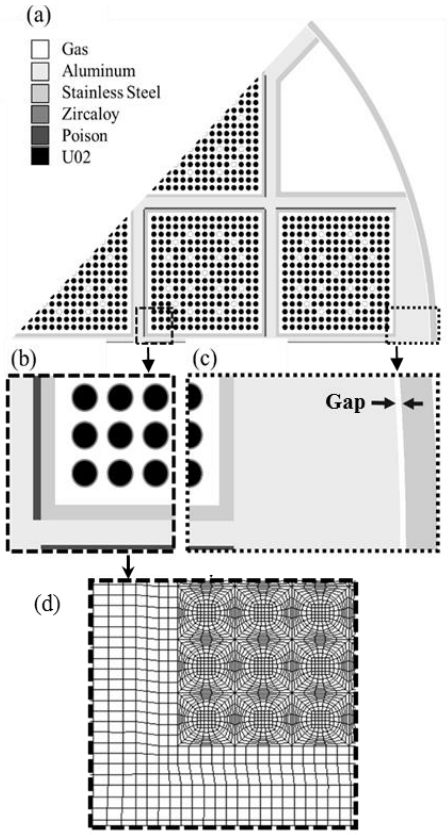

Fig. 3. Regional materials and mesh details of computational domain. (a) Grey scale coded material list for the model. (b) Detailed region of the fuel rod array in the stainless steel basket. (c) Detailed view of the 2.29 mm annular gap that surrounds the entire canister. (d) Mesh detail of the region (b).

and represents the smallest dimension in the canister with size of 2.29 mm.

The outer diameter of each rod measures 10.92 mm with a 0.67 mm Zircaloy sheath. The rod center-to-center pitch is 14.43 mm. The 2D reference depth used in the model is 3.66 m. The domain shown in Figure 3 with the detailed view of the region (b) (Figure 3d) contains a total of 131,202 elements.

Steady-state and transient thermal simulations were performed using ANSYS/Fluent 15. These simulations assume uniform heat generation in all the UO_2 regions at given axial location, and they included conduction within the solids and gas regions, and surface-to-surface radiation across the gas regions with surface emissivity of 0.46 for the stainless steel and 0.8 for the aluminum and zircaloy [27]. These simulations do not include buoyancy-induced gas motion or natural convection in the backfilled regions because they are negligible at the pressures considered in this work. The outer boundary condition of the transfer cask is assumed to be underwater at a constant temperature of 101.7°C. This boundary condition is used for all the simulations (steady-state and transient simulations)

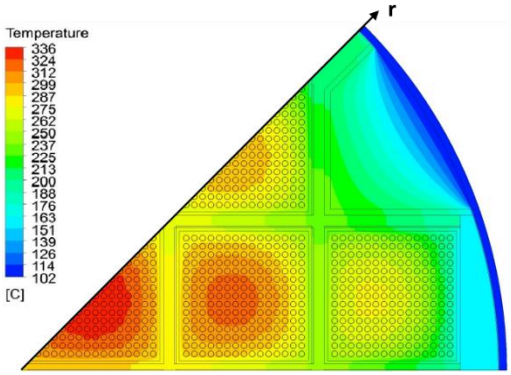

Fig. 4. Temperature contour plots (helium at atmospheric pressure with Q=2291 W/m/assembly)

reported in this paper. The heat input for each fuel rod region is 270 to 1000 W/m/assembly, calculated as

$$Q' = P_f \frac{Q}{L} \tag{12}$$

where P_f and L are the axial peaking factor and the length of the fuel rods. The value of 1.1351 for the peaking factor is used [28]. Q is the total heat generated per fuel assemblies.

V. RESULTS AND DISCUSSION

Two different heat transfer models are used in this work. The first is the continuum model, which does not include temperature jumps at the interface between solid surfaces and helium. The second is the temperature jump model, which includes the Willis-temperature-jump-thermal-resistance model described in equations (5) and (8). Simulations for this model are performed for pressure P=100 Pa, and thermal accommodation coefficients α=0.2, 0.4 and 1.

Figure 4 shows temperature contours from the continuum model (P=1 atm) with outer enclosure wall temperature at 101.7°C and heat generation of 2291 W/assembly. The maximum peak cladding temperature in the domain is located in the center of the innermost fuel assembly. The maximum peak temperature obtained is T_P=336.3°C which below the allowable maximum clading temperature T_{RH}=400°C.

Figure 5 shows the profile of the temperature along the r-axis shown in Figure 4 for the continuum and temperature jump models. The highest temperatures in the domain are located at the center of the assemblies and the minimum temperatures are located at the outer assembly regions. The temperatures within the fuel rods are relatively uniform compared to the gas region between solids. For the continuum model (solid line) sudden increase of temperature occurred at the gap between the aluminum support and stainless-steel-enclosure (see Figure 3). This is due to the low thermal conductivity of helium when compared to aluminum and stainless steel, and also to the accumulation of heat generated by the fuel rods in this gap. The effect of radiation heat transfer is weak since the

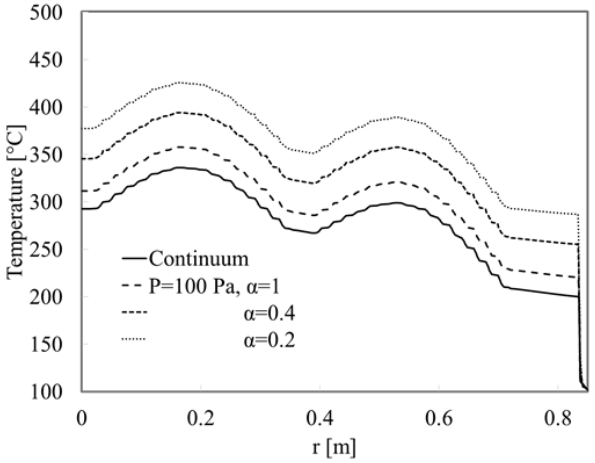

Fig. 5. Radial temperature profile along the radial axis shown in Figure 5, calculated for Q=2291 W/ assembly and for continuum model (atmospheric pressure) and temperature jump model (P=100 Pa) for different values of the thermal accommodation coefficient.

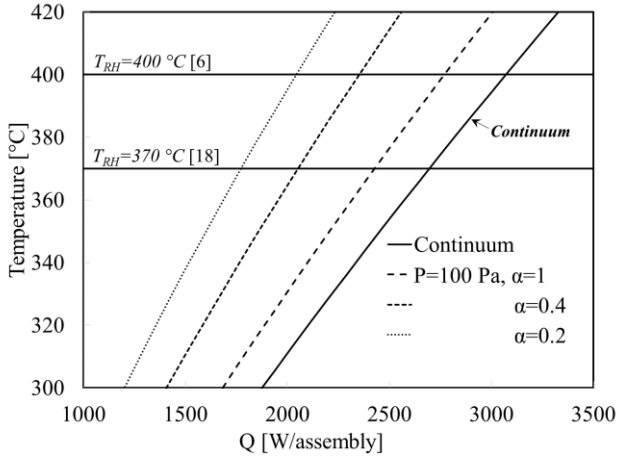

Fig. 6. Peak cladding temperature versus fuel heat generation rate for helium at atmospheric pressure (continuum model) and P=100 Pa (temperature jump model) with three values of the thermal accommodation coefficient α=1, 0.4 and 0.2.

temperatures in the gap are relatively small. The maximum temperature reached for the continuum model is less than the limit temperature of 400°C. The continuum model is valid down to the pressure of 13,345 Pa, which represents the limit between the continuum and slip regime (Kn=10^{-3}). Below this pressure the effects of gas rarefaction start to be visible.

Figure 5 shows also the results for the temperature jump model (P=100 Pa). When the pressure in the domain decreases from atmospheric pressure to P=100 Pa the maximum temperature in the domain increases. The same behavior is observed when the thermal accommodation coefficient (α) decreases while the pressure is kept constant at P=100 Pa. The maximum temperature jump is induced at the gap between the aluminum support and stainless-steel-enclosure. The participation of the fuel cladding surfaces in the increase of the temperature due to temperature jump resistance is small. For the case P=100Pa and α=0.2 the maximum peak cladding temperature is T_P=425.8°C, which is higher by 89.5°C comparing to the continuum model and exceed the allowable limit T_{RH}=400°C. This shows the importance of taking into account the effects of rarefied gases for the estimation of the peak cladding temperature during vacuum drying operations. It should be noted that the pressures during vacuum drying operations may be less than 100 Pa (around 70 Pa), which has the potential to further increase the cladding's temperature.

Figure 6 shows the maximum peak cladding temperature as function of the fuel heat generation per assembly. The results are reported for atmospheric pressure conditions (continuum model) and for P=100 Pa (temperature jump model) with three values of the thermal accommodation coefficient α=1, 0.4 and 0.2. The temperature limit that leads to the formation of radial hydride considered in the United States (T_{RH}=400°C) and in Germany ($T_{RH,R}$=370°C) are shown by two horizontal lines.

The temperature differences between the temperature jump and continuum models increase as the heat generation increases. For a given heat generation this difference can be higher than 80°C. The temperatures experienced with the temperature jump model are always higher than those with the continuum model. Smaller value of thermal accommodation coefficient α leads to higher temperature.

From Figure 6 the maximum allowable heat generation that brings the peak cladding temperature to the radial hydride formation temperature T_{RH}=400°C and the reduced one $T_{RH,R}$=370°C are obtained and the values are given in Table I.

TABLE I. Maximum allowable heat generation per assembly Q for continuum model (P=1 atm) and temperature jump model (P=100 Pa) at the radial hydride formation temperature T_{RH}=400°C and the reduced temperature $T_{RH,R}$=370°C.

Temperature of radial hydride formation	Maximum heat generation [W/assembly]			
	Continuum model	Temperature jump model		
		α=1	α=0.4	α=0.2
T_{RH} = 400°C	3070	2769	2351	2043
$T_{RH,R}$ = 370°C	2695	2426	2051	1772

Table I shows that the maximum allowable heat generations predicted by the continuum model are higher than those predicted by the temperature jump model. For the case of temperature jump model (P=100 Pa) with α=0.2 the maximum allowable heat generation that brings the peak cladding temperature to the limit of 400°C is 34% less than that predicted by the continuum model.

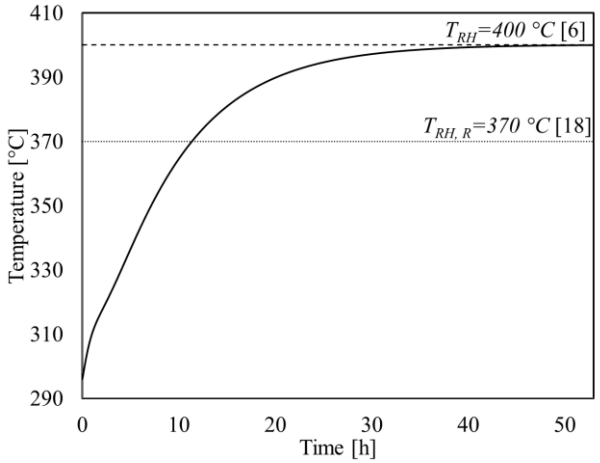

Fig. 7. Transient response of the fuel assemblies under vacuum drying condition. Peak cladding temperature as function of time.

Figure 7 shows the transient response of the fuel assemblies subjected to vacuum drying. The maximum peak cladding temperature in the domain is plotted versus the time in hours. The fuel assembly heat generation Q=2351 W/assembly that brings the peak cladding temperature to the limit of 400 °C is used (see Table I).

The transient simulation is performed in two steps. First, steady state simulation is performed with canister/cask filled with water, which simulate the condition of loading the fuel assemblies into the canister while it is underwater. Second, the transient simulation is started by using the temperature field from the steady state simulation as an initial condition. The pressure during the transient simulation is set to the vacuum pressure P=100 Pa and the value of thermal accommodation coefficient α=0.4 is used.

At the beginning of transient simulation the maximum cladding temperature in the domain is T_P=297.4°C. The maximum cladding temperature increases with time and reaches the limit of 400°C within 53 hours. This time is less than the typical time for vacuum drying of a canister with BORAL® neutron poison, more than 60 hours [29]. The time needed to reach the limit temperature of 370°C, used in Germany, is 11.5 hours. For fuel assemblies with heat generation 10 % higher than Q=2351 W/assembly the time to reach the limit temperature of 400°C decreases significantly, t=13.75 hours, for the same conditions of pressure and thermal accommodation coefficient. It should be noted here that the value of the accommodation coefficient is kept constant for the transient simulation. However, its value varies with temperature, as temperature increases the value of the thermal accommodation coefficient decreases [24]. This has the potential to further increase the temperature and reduce the time to reach the limit temperature.

Figure 7 shows also that at the beginning of the simulation, below 5 hours, there is a bump in the profile of temperature. At the starting of the simulation the temperatures in the domain are low and the heat is mainly transferred by conduction through solid and gas. As the temperature increases the portion of heat transferred by radiation becomes more important, which results in the changing of the temperature slope. Another reason could be the change of location of the maximum temperature within the innermost fuel assembly.

VI. CONCLUSIONS

Geometrically-accurate-two-dimensional simulations of heat transfer in used nuclear transfer cask containing 24 assemblies of 15×15 fuel rods array have been performed using ANSYS/Fluent code. Steady state and transient simulations were performed to calculate the peak cladding temperatures during vacuum drying conditions of the transfer cask filled with helium at atmospheric pressure (continuum model) and P=100 Pa (temperature jump model).

ANSYS/Fluent simulations in simple geometries (parallel plate and concentric cylinders) were compared to the accurate DVM kinetic model based on the Boltzmann equation [20] for different values of the thermal accommodation coefficient in order to assess the accuracy of ANSYS/Fluent to model the conditions of gas rarefaction. The simulation results showed that the Willis model for temperature jump applied in ANSYS/Fluent was in good agreement with the DVM kinetic calculations. This model was applied for the transfer cask simulations.

For the steady state simulations of the transfer cask, the continuum model (which did not include the temperature jump effect) was compared to the temperature jump model at P=100 Pa. The results showed that the peak cladding temperature in the domain is located in the center of the innermost fuel assembly. When the temperature jump model was applied, with thermal accommodation coefficient α=1, the peak cladding temperature increased by 21.5°C comparing to the continuum model. The change of the thermal accommodation coefficient from 1 to 0.2 caused an increase of temperature of 89.5°C when compared to the continuum model. The results showed also the gap between the aluminum support and stainless-steel-enclosure plays the more important role in temperature increase. The heat generation rate that causes the radial hydride formation predicted by the temperature jump model was 34% less than that predicted by the continuum model.

The transient simulation results showed that the required time to reach the maximum peak cladding temperature T_{RH}=400°C is 53 hours for the vacuum conditions of P=100 Pa and α=0.4. A slight increase of the fuel assembly's heat load could significantly reduce this time. A change of thermal accommodation coefficient α from 0.4 to 0.2 also has the potential to significantly reduce this time.

This paper showed that taking into account of the effect of gas rarefaction in the simulations of the vacuum drying operations is crucial to accurately model this process, as it results in significant increase of temperature, which is not considered in the continuum model.

ACKNOWLEDGMENTS

This work was supported by the US Department of Energy Office of Nuclear Energy University Program.

REFERENCES

1. Holtec International, "HI-STORM 100 FSAR", Revision 8, Report HI-2002444, (2010).
2. D. Colmont and P. Roblin, "Improved thermal modeling of SNF shipping cask drying process using analytical and statistical approaches," *Packaging, Transport, Storage & Security of Radioactive Material*, vol. 19, no. 3, pp. 160-164, (2008).
3. P. Loscoe, "Transitioning metallic uranium spent nuclear fuel", *WM'00 Conference*, Tucson, AZ, (2000).
4. R. Wittman, "Radiolysis model sensitivity analysis for a used fuel storage canister", U.S Department of Energy. PNNL-22773, (2013).
5. B. Hanson, H. Alsaed, C. Stockman, D. Enos, R. Meyer and K. Sorenson, "Gap Analysis to Support Extended Storage of Used Nuclear Fuel", FCRD-USED-2011-000136 Rev. 0, U.S. Department of Energy Used Fuel Disposition Campaign, (2012).
6. "Cladding Considerations for the Transportation and Storage of Spent Fuel", ISG-11 R3, Interim Staff Guidance Report for the Spent Fuel Project Office of the U.S. NRC, (2003).
7. R. S. Daum, S. Majumdar and M. Billone, "Experimental and Analytical Investigation of the Mechanical Behavior of High-Burnup Zircaloy-4 Fuel Cladding", J. ASTM Intern., vol. 5, no. 5, (2008).
8. R. S. Daum, S. Majumdar, Y. Liu and B. M.C., "Radial-hydride Embrittlement of High-burnup Zircaloy-4 Fuel Cladding", J. Nucl. Sci. Tech., vol. 43, no. 9, pp. 1-14, (2006).
9. M. C. Billone, T. Burtseva and R. Einziger, "Ductile-to-brittle transition temperature for high-burnup cladding alloys exposed to simulated drying-storage conditions", J. Nucl. Mater, vol. 433, pp. 431-448, (2013).
10. M. C. Billone, T. Burtseva and Y. Liu, "Baseline Properties and DBTT of High-Burnup PWR Cladding Alloys," in Proc. PATRAM, San Francisco, CA, (2013).
11. W.S. Large, and R.L. Sindelar, "Review of Drying Methods for Spent Nuclear Fuel", Westinghouse Savannah River Company, Savannah River Site, Aiken, SC, report number WSRC-TR-0075, (1997).
12. L. Loeb, Kinetic Theory of Gases, 2nd Edition, McGraw-Hill Book Company Inc., (1934).
13. E. H. Kennard, Kinetic Theory of Gases, McGraw-Hill Book Company, Inc., New York, (1938).
14. S. A. Schaaf and P. L. Chambre, Flow of Rarefied Gases, Princeton University Press, (1961).
15. Y.S. Tseng, J.R. Wang, F.P. Tsai, Y.H. Cheng and C. Shih, "Thermal design investigation of a new tube-type dry-storage system through CFD simulations", Annals of Nuclear Energy, 38, 1088-1097, (2011).
16. Holtec International, "Topical Report on the HI-STAR/HI-STORM Thermal Model and its Benchmarking with Full-Scale Cask Test Data", Holtec Report No. HI-992252, (2000).
17. Pacific Northwest Laboratory, "The TN-24P PWR Spent Fuel Storage Cask: Testing and Analyses", EPRI NP-5128, (1987).
18. H. G. Kim, Y. H. Jeong, and K. T. Kim, "The effects of creep and hydride on spent fuel integrity during interim dry storage", Nuclear Engineering and Technology, vol.42 no.3, (2010).
19. G. A. Bird, "Definition of mean free path for real gases", Phys. Fluids, 26, 11, (1983).
20. I. Graur, M. T. Ho and M. Wuest, "Simulation of the transient heat transfer between two coaxial cylinders", J. Vac. Sci. Technol. A 31(6) (2013).
21. G. A. Bird, Molecular Gas Dynamics and the Direct Simulation of Gas Flows. Oxford Science Publications, (1994).
22. J. C. Maxwell, "On stress in rarefied gases arising from inequalities of temperature," Phil.Trans. R. Soc. Lond., vol. 170, p. 231–256, (1878).
23. F. O. Goodman, "Thermal accommodation coefficients", J. Phys. Chem. 84, 1431-144, (1980).
24. S. Song, and M. M. Yovanovich, "Correlation of thermal accommodation coefficient for 'engineering' surfaces", Proceedings of the 24th ASME National Heat Transfer Conference and Exhibition, Pittsburgh, PA, pp. 107-116, (1987).
25. F. Sharipov, "Data on the velocity slip and temperature jump coefficients", Thermal and Mechanical Simulation and Experiments in Micro-Electronics and Micro-Systems. Proc. 5th Int. Conf. EuroSimE, Belgium, pp. 243-249, (2004).
26. J. T. Lin and D. R. Willis, "Kinetic Theory Analysis of Temperature Jump in a Polyatomic Gas," *Phys. Fluids*, vol. 15, p. 31 (1972).
27. M. F. Modest, Radiative Heat Transfer, 2nd Edition, Academic Press, New York (2003).
28. R. H. Bahney, and T. L. Lotz, Spent Nuclear Fuel Effective Thermal Conductivity Report, Prepared for the U.S. DOE, Yucca Mountain Site Characterization Project Office by TRW Environmental Safety Systems, Inc., (1996).
29. W. Bracey and P. Smith, "Transnuclear Drying Experience and Lessons Learned," ASTM Workshop, Atlanta, GA, (2012).